Applied Catalysis B: Environmental 160–161 (2014) 286–297

Contents lists available at ScienceDirect

Applied Catalysis B: Environmental

journal homepage: www.elsevier.com/locate/apcatb

Deleterious effect of homogeneous and heterogeneous near-neutral photo-Fenton system on *Escherichia coli*. Comparison with photo-catalytic action of TiO_2 during cell envelope disruption

C. Ruales-Lonfat[a], N. Benítez[b], A. Sienkiewicz[c], C. Pulgarín[a,*]

[a] SB, ISIC, GPAO, Station 6, Ecole Polytechnique Federal de Lausanne, 1015 Lausanne, Switzerland
[b] Universidad del Valle, Grupo de Investigación en Procesos Avanzados de Oxidación (GAOX), Cali A.A. 25360, Colombia
[c] SB, IPMC, LPMC, Station 3, Ecole Polytechnique Federal de Lausanne, 1015 Lausanne, Switzerland

ARTICLE INFO

Article history:
Received 12 November 2013
Received in revised form 28 April 2014
Accepted 3 May 2014
Available online 10 May 2014

Keywords:
Near-neutral photo-Fenton
TiO_2 photocatalysis
E. coli inactivation
Lipid peroxidation
ONPG hydrolysis test

ABSTRACT

The mechanisms underlying bacterial inactivation by solar photo-Fenton at near-neutral pH have not yet been investigated in detail. In particular, no consensus exists on the bacterial inactivation mechanism under solar light enhanced by the Fenton's reagents (Fe^{3+}, H_2O_2). In this study, cell envelope damage during bacterial inactivation by near-neutral photo-Fenton and TiO_2 photocatalysis were comparatively studied using lipid peroxidation and cell permeability change indicators. TiO_2 photocatalysis was found to result in marked cell envelope damage, in contrast to the near-neutral photo-Fenton process. However, similar kinetics of inactivation were observed for both types of processes. This finding corroborated with the results of an electron spin resonance (ESR) study, which pointed to higher efficiency of photogeneration of reactive oxygen species (ROS) in the presence of TiO_2 photocatalyst compared with the photo-Fenton system at near-neutral pH. In the context of the photo-Fenton processes, the bactericidal effect of $Fe^{3+}/h\nu$ was attributed to the adsorption of Fe^{3+} ions on the bacterial cell wall and the subsequent photosensitization of these iron-bacteria exciplexes, thus leading to the direct oxidation of the cell membrane. In contrast, the effect of $Fe^{2+}/h\nu$ was associated with diffusion into the cell by the FeO system and its participation in intracellular dark Fenton's reactions.

Based on these experimental results and literature reports, a mechanistic interpretation of the photoinactivation of *Escherichia coli* in the presence of Fe^{2+}, Fe^{3+}, and the Fenton's reagent is proposed. Moreover, we suggest that extensive cell envelope damage might not necessarily be a unique pathway in bacterial inactivation by near-neutral photo-Fenton treatment. In particular, the enhancement of an internal (photo)-Fenton process by the synergistic action of UVA and the external Fenton's reactants seems an important contribution to bacterial inactivation.

1. Introduction

Harmful microorganisms are a major problem in drinking water that can cause severe health problems for humans. Hence, developing innovative water disinfection methods is a continuous need. Recently, the photo-Fenton ($Fe^{2+}/^{3+}/H_2O_2/h\nu$) system at near-neutral pH under solar light was found to be an effective option for disinfection of bacteria present in water [1–3]. Fenton's reagent action is based on the reaction of H_2O_2 with $Fe^{2+}/^{3+}$, thus resulting in the formation of hydroxyl radicals ($^{\bullet}OH$) and other highly oxidative species in aqueous media (Eqs. (1) and (2)). However, the Fenton process is limited by the Fe^{2+} regeneration of Fe^{3+} (Eq. (2)). This drawback is partially countered by photo-Fenton reactions. In fact, Fe^{3+}-hydroxy complexes undergo photo-reduction under ultraviolet A (UV-A) and visible radiation, thus regenerating Fe^{2+} *via* ligand-to-metal charge transfer (LMCT) and contributing to an additional pathway of $^{\bullet}OH$ production (Eq. (3)) [4].

$$Fe^{2+} + H_2O_2 \rightarrow Fe^{3+} + {}^{\bullet}OH + OH^- \quad k = 53\text{–}76\,M^{-1}\,s^{-1} \tag{1}$$

$$Fe^{3+} + H_2O_2 \rightarrow Fe^{2+} + HO_2{}^{\bullet} + H^+ \quad k = 1\text{–}2 \times 10^{-2}\,M^{-1}\,s^{-1} \tag{2}$$

$$Fe(OH)^{2+} + h\nu \rightarrow Fe^{2+} + {}^{\bullet}OH \tag{3}$$

$$[Fe(COO{-}R)]^{2+} + h\nu \rightarrow Fe^{2+} + CO_2 + R^{\bullet} \tag{4}$$

Until now, the process pH was generally perceived as the limiting factor for photo-Fenton systems, because $Fe(OH)^{2+}$ the

* Corresponding author. Tel.: +41 21 693 47 20; fax: +41 21 693 6161.
E-mail address: Cesar.pulgarin@epfl.ch (C. Pulgarín).

http://dx.doi.org/10.1016/j.apcatb.2014.05.001
0926-3373/

most photo-active Fe^{3+}-hydroxy complex is predominant at low pH (~2.8). At near-neutral pH, zero-charge ferrous complexes [$Fe(OH)_2$] formed, are very sensitive to oxidation and instantaneously form solid ferric (hydr)oxide compounds such as magnetite, goethite, lepidocrocite, or feroxyhyte. The type of precipitated ferric compounds depends on physico-chemical conditions such as acidity, redox conditions, temperature, ionic strength, presence of organic or inorganic ligands and bacterial activity [5]. In waters containing dissolved organic matter (DOM), Fe^{3+} may complex with certain of these organic compounds. The Fe^{3+}-organo complexes are stable at neutral pH, circumventing the need for the low pH of the standard photo-Fenton process. The photolysis of these Fe^{3+}-organo complexes, which generally have a high molar absorption coefficient in UV-A and visible light, leads to the regeneration of Fe^{2+} and the formation of a ligand radical [6] (Eq. (4)). Both Fe^{2+} and organic radicals react with O_2, leading to the formation of reactive oxygen species (ROS) ($O_2^{\bullet-}$, $^{\bullet}OH$, H_2O_2) [7,8].

Over the past few years, interest has grown in the application of near-neutral photo-Fenton treatment to inactivate larvae of freshwater mollusc (zebra mussel) [9] and other types of microorganisms such as fungi [10], virus [11] and *Enterococcus faecalis* [12]. However, the mechanism underlying the photocatalytic inactivation process has not been investigated in detail. Many studies on elucidating the mechanism of photo-killing of bacterial cells using TiO_2 concluded that cell envelope damage is the first and perhaps a major step for microbial inactivation. Sunada et al. [13] proposed that bacterial death is caused by a significant disorder in cell permeability and the decomposition of the cell wall [14]. More specifically, Maness et al. and Pulgarin et al. [15–17] concluded that TiO_2 photocatalysis promotes the peroxidation of the phospholipids in the membrane. More recently, Dalrymple et al. [18] reported that lipid peroxidation processes are crucial to *Escherichia coli* inactivation using TiO_2 suspension and UVA light sources.

For the first time, this study investigates cell envelope damage during *E. coli* inactivation by the near-neutral photo-Fenton system and compares the underlying mechanisms with the photocatalytic action of TiO_2. The production of malondialdehyde (MDA) was used as an index to assess cell membrane damage by lipid peroxidation, and the ortho-nitrophenyl-β-D-galactoside (ONPG) test was used as an index of cell permeability. To confirm the effect of both types of photo-oxidative treatment on the bacterial wall, lipopolysaccharide (LPS), an essential compound of the cell wall of *E. coli*, was used as a model. Furthermore, bacterial inactivation by $FeSO_4$ and goethite-based photo-Fenton systems at near-neutral pH were comparatively studied to evaluate homogeneous and heterogeneous contributions to the bacterial inactivation mechanism.

Lipid peroxidation during photo-assisted Fe^{2+}/Fe^{3+} treatment and its correlation with bacterial inactivation were also assessed. Finally, based on our results and literature reports, a scheme of the effects of the Fe^{2+}/Fe^{3+} and the Fenton's reagents on photoinactivation of bacteria was proposed.

2. Materials and methods

2.1. Chemicals

This study used the commercial mixed-phase TiO_2-based photocatalyst, Degussa P25 (Frankfurt, Germany) as a high-activity model photocatalyst. Degussa P25 is composed of anatase and rutile crystallites (typical reported ratio of 75:25), having irregular shapes and average particle sizes of 20–30 nm. The specific surface area of TiO_2 particles is 50 m^2/g. The reactants used for the Fenton process were ferrous sulphate heptahydrate ($FeSO_4 \cdot 7H_2O$) (Riedel-de Haën 99–103.4%), and iron chloride ($FeCl_3 \cdot 6H_2O$) (Fluka, Buchs, Switzerland); experiments with iron oxide were carried out using granular goethite (α-FeO(OH), 30–50 mesh (Sigma–Aldrich South Africa) and hydrogen peroxide (H_2O_2) 30% w/v (Riedel de Haën, Darmstadt, Germany). The lipopolysaccharide (LPS) FITC from *E. coli* 055:B5 (Code F8666) and ortho-nitrophenyl-β-D-galactoside (ONPG) were purchased from Sigma Aldrich and used without further purification. LPS was dissolved in Milli-Q water (0.4 mg/mL). With a lower concentration, no malondialdehyde (MDA) signal was detected using HPLC. All solutions were prepared using Milli-Q water (18.2 MΩ cm) immediately before irradiation.

2.2. Analytical methods

2.2.1. Dissolved iron

Dissolved iron ($Fe^{2+/3+}$) was measured using the Ferrozine method as described previously [19]. Total dissolved iron was measured using an Inductively Coupled Plasma Emission Spectrometer (ICP) (Shimadzu) ICPE-9000. Samples were filtered (0.25 μm) and kept in acid solution previous to the determination. The detection limit of ICPE used for this experiment was 0.2 μg/L.

2.2.2. Analysis of H_2O_2 concentration

The concentration of H_2O_2 was monitored using a titanium (IV) oxysulfate solution *via* a spectrophotometric method at 410 nm (modified method DIN 38 402 H15). The titanium (IV) oxysulfate method has a 0.1 mg/L detection limit.

2.2.3. Electron spin resonance spectroscopy (ESR)

Electron spin resonance spectroscopy (ESR) in combination with spin-trapping were used to monitor the formation of reactive oxygen species (ROS), in other words, hydroxyl ($^{\bullet}OH$) and superoxide ($O_2^{\bullet-}$) radicals, generated by either the near-neutral photo-Fenton processes or under the photo-catalytic action of TiO_2 particles. A commercial spin trap, 5,5-dimethyl-1-pyrroline-N-oxide (DMPO), from Sigma–Aldrich (Buchs, Switzerland) was used to trap ROS. DMPO was purified before use through distillation on activated charcoal. Then, a stock solution of 0.5 M DMPO in ultrapure water (Milli-Q) was stored at −20 °C.

The following reagents studying the photo-generation of ROS using the near-neutral photo-Fenton system: 3.8 mg/L of iron ($FeSO_4$ or goethite) and 10 mg/L of H_2O_2. To study the formation of ROS under the photo-catalytic action of TiO_2, the aqueous suspension containing 1 mg/mL of TiO_2 particles in Milli-Q water was prepared. Just before performing the photo-generation of ROS, DMPO (100 mM) was added to Fenton's reagents or aqueous suspensions containing TiO_2. Subsequently, 1 mL aliquots of the prepared samples were transferred into small Pyrex beakers (5 mL volume, 20 mm outer diameter and 30 mm height) and exposed to simulated solar light (intensity 1322 W/m^2) under constant agitation.

Subsequently, the solutions of either the Fenton's reagents or the water suspensions of TiO_2 particles were drawn into thin glass capillaries (0.7 mm ID/0.87 mm OD, from VitroCom, NJ, USA), which were then sealed on both ends using the Cha-Seal™ tube-sealing compound (Medex International, Inc., USA). ESR measurements were carried out at room temperature using a Model EleXsys 500 Bruker X-band spectrometer (Bruker BioSpin, Karlsruhe, Germany) equipped with a high-Q cylindrical TE_{011} microwave cavity, Model ER4123SHQE. The instrumental settings were: frequency of 9.4 GHz; microwave power of 0.63 mW; scan width of 120 G; magnetic field resolution of 2048 points; modulation frequency of 100 kHz; modulation amplitude of 1.0 G; receiver gain of 60 dB; conversion time of 40.96 ms; time constant of 20.48 ms and sweep time of 84 s.

The spin-adducts concentrations were measured using double-integration of the first-derivative ESR spectra. The resulting areas were compared with the ESR signal from 10 μmol/L of a stable

nitroxide radical, 4-hydroxy-2,2,6,6-tetramethylpiperidine 1-oxyl (TEMPOL, Sigma–Aldrich, Switzerland). The data analysis was carried out using Origin Pro 9.0 software.

2.3. Bacterial strains and growth media

The bacterial strain used was *E. coli* K12 (MG1655), a non-pathogenic wild-type strain that can be handled with little genetic manipulation. Bacteria was inoculated from a stock in Luria–Bertani (LB) and incubated at 37 °C and 180 rpm in a shaker incubator. After 8 h, cells were diluted (1%, v/v) in pre-heated LB broth and incubated at 37 °C for 15 h in the incubator until a stationary physiological phase was reached. Cells were separated during the stationary growth phase by centrifugation (15 min at 5000 rpm and 4 °C). The bacterial pellet was resuspended and washed for 10 min in the centrifuge (twice). This procedure resulted in a bacterial pellet of approximately 10^9 colony forming units per milliliter (CFU/mL).

2.4. Photo-inactivation experiments

Six circular Pyrex reactors (4 cm × 9 cm, 100 mL) were placed on a magnetic stirrer in a solar simulator (CPS Suntest System Heraeus Noblelight, Hanau, Germany). The Suntest System contained a basic uncoated quartz glass light tube with a filter E and an IR screen (to simulate solar global radiation from outdoor daylight). The temperature in the reactors was <38 °C and the radiance intensity was 1322 W/m^2 (20 W/m^2 UV-A).

At the beginning of each experiment, the Pyrex reactors containing the bacterial suspension in Milli-Q water (approximately 10^6–10^8 CFU/mL) were placed in the dark at 25 °C under magnetic stirring for at least 30 min to let the bacteria adapt to the new matrix and to allow the die-off and equilibration of the most stress sensitive species. Then, Fenton's or TiO_2 reagents were added and exposed to irradiation. Aliquots were taken during set intervals within the inactivation time. The control experiment consisted of an *E. coli* suspension without reagents. Concentrations were set as follows: photo-Fenton ($Fe^{2+}/^{3+}$ 0.6 mg/L, H_2O_2 10 mg/L), and TiO_2 photocatalysis (1 mg/mL). These concentrations are in the optimal range reported in the literature for photo disinfection studies [19]. Bacterial reactivation and/or growth of bacteria was determined for some experiments by leaving the last samples in the dark at room temperature (20–25 °C) for 24 h before the measurement of the CFU.

2.5. Determination of lipid peroxidation

Lipid peroxidation level was measured using the accumulation of malondialdehyde (MDA) and quantified through high performance liquid chromatography (HPLC) after both photo-oxidative treatment methods on *E. coli* and LPS [20]. Briefly, chromatographic determinations were performed on an Agilent 1100 series HPLC equipped with a UV absorbance detector. Samples filtered were injected *via* autosample and eluted at a flow rate of 0.9 mL/min through a column (Nucleosil C18, Marcherey-Nagel) using as mobile phase a mixture of 3 mM de KH_2PO_4–MeOH (65 + 35%, v/v) at pH 4. Chromatograms were monitored at 268 nm and the retention time of MDA was 3.9 min. For calibration purposes, a solution of MDA was prepared through acid hydrolysis of 1,1,3,3-tetraethoxypropane, as in Tsaknis et al. [21].

2.6. Damage in cell envelope by photo-Fenton and TiO_2 photocatalysis

Ortho-nitrophenyl-β-D-galactoside (ONPG) is a synthetic chromogenic substrate for the intracellular β-D-galactosidase of *E. coli* that can be used to gauge the level of cellular damage during the photocatalytic process and assess to it any correlation of cell death. ONPG is hydrolyzed to *o*-nitrophenol (ONP) when it reacts with β-D-galactosidase, which results in a yellow color under alkaline conditions. The production of ONP over time was monitored using a spectrophotometer at 420 nm. This assay was carried out as described by Huang et al. [22], with minor modifications. In order to enhance the synthesis of β-D-galactosidase by *E. coli*, the following culturing method was employed. *E. coli* grown in LB Broth for 18 h at 37 °C was further spiked to a flask containing 1 mM of isopropyl β-D-thiogalactopyranoside and 100 mL of LB Broth. After incubation for 4 h at 32 °C in a shaking incubator, the suspension was centrifuged at 4500 rpm for 10 min at 4 °C and washed using Milli-Q water.

The hydrolysis rate for intact and lysed cells was determined. An aliquot of 9 mL washed cells was mixed with 1 mL ONPG (5 mM in sterile Milli-Q water) then, 0.9 mL samples were transferred to sterile Eppendorf tube. Each 3 min interval for 12 min, 0.1 mL of a 1 M sodium carbonate/bicarbonate buffer (pH 10) was added to both stop the enzyme-substrate reaction and to obtain maximal absorbance. The kinetics was determined by following the absorbance of the samples and the slope was determined by linear regression of absorbance *versus* time.

A sample from the photocatalytic experiments were taken at 15 min intervals for 120 min in duplicate. The ONPG hydrolysis reactions were initiated by transferring 4.5 mL of illuminated samples to the dark in duplicates in a tube, followed by an addition of an equal volume of Milli-Q water and 1 mL of ONPG. TiO_2 and cells were removed by centrifugation at 4 °C and 4500 rpm for 10 min. Exceeding H_2O_2 was neutralized with catalase for photo-Fenton treatment. The pH of the supernatant was raised to 10 by the addition of a sodium carbonate/bicarbonate buffer. The absorbance of the mixture was measured at 420 nm and the hydrolysis rate was determined as described in Section 2.6.

The effect of TiO_2 photocatalyst and photo-Fenton treatment on cell-free β-D-galactosidase was examined using cell lysate. An aliquot of 2 mL washed cell was transferred in a beaker and followed by the addition of 50 μL chloroform and vigorous stirring for 15 min. This solution was then diluted 1:10 in Milli-Q water and subjected to TiO_2 photocatalytic and photo-Fenton treatment as described before in this section. The illuminated cell lysates were transferred to the dark at 15 min intervals for 120 min followed by the ONPG assay as described above.

3. Results and discussion

3.1. Comparative bacterial inactivation mechanisms under near-neutral photo-Fenton and TiO_2 photocatalysis

To determine cell wall damage in *E. coli*, lipid peroxidation was monitored through accumulation of MDA, one of the most abundant aldehyde forms originating from the peroxidation of bacterial lipid membranes [23,24]. As Fig. 1a (traces (▲) and (♦)) shows, even though MDA accumulation was low for both TiO_2 photocatalysis and near-neutral photo-Fenton treatment before 120 min, this effect was nevertheless sufficient to induce a significant bacterial inactivation, a ~5 $\log_{10}$ reduction (99.99%) of the initial *E. coli* concentration as shown in Fig. 1b (traces (▲) and (♦)). Thus, *E. coli* inactivation, monitored by the cultivability measurements in petri dishes, does not correlate in time with the appearance of MDA. This low MDA accumulation before 120 min can be explained by (i) limited peroxidation (not noticeable by significant MDA accumulation), which is enough to induce cultivability losses, and (ii) the contribution of other parallel processes that lead to physiological perturbations related to the attack of cell wall components. At a

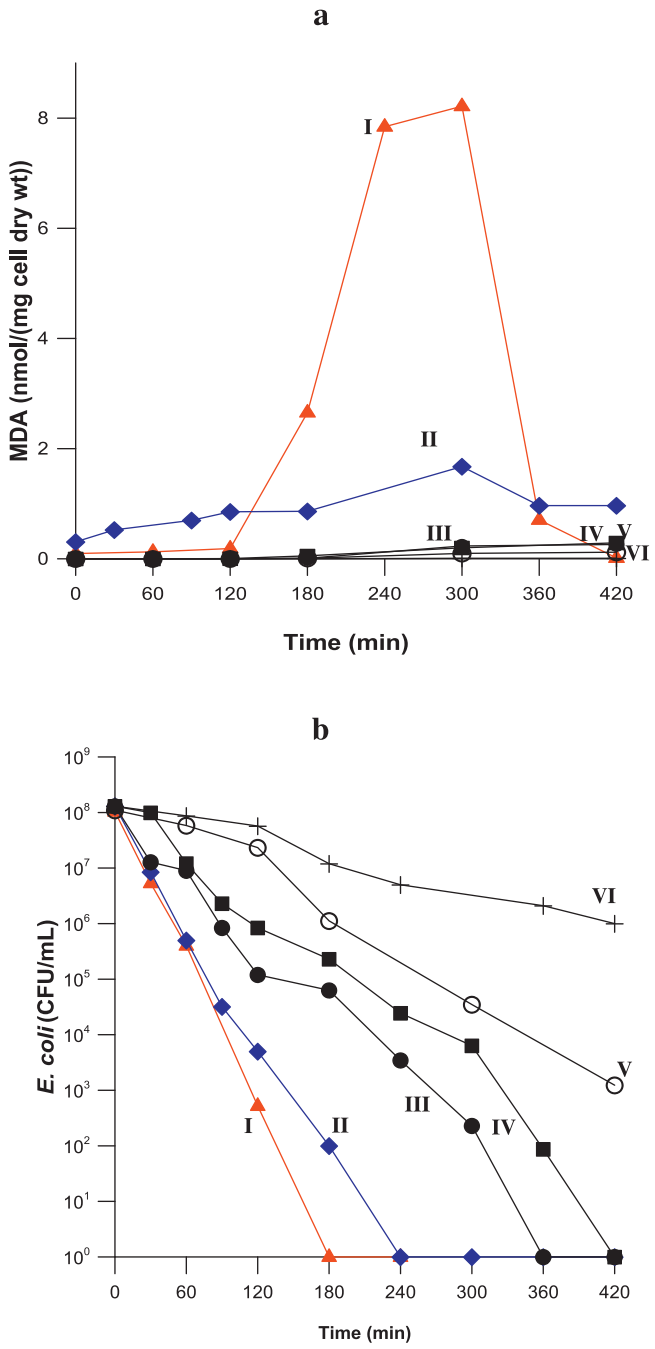

Fig. 1. (a) Lipid peroxidation based on MDA accumulation and (b) *E. coli* inactivation during: (I) (▲) TiO_2 photocatalysis (1 mg/mL); (II) (♦) photo-Fenton ($FeSO_4$ (Fe^{2+} 0.6 mg/L), H_2O_2 (10 mg/L), under light); (III) (●) $FeSO_4$ (Fe^{2+} 0.6 mg/L), under light; (IV) (■) H_2O_2 (10 mg/L), under light; (V) (○) light alone; (VI) (+) Fenton ($FeSO_4$ (Fe^{2+} 0.6 mg/L), H_2O_2 (10 mg/L). Experiments were conducted in triplicate and standard error was found to be approximately 5%.

more advanced stage of treatment (up to 120 min, Fig. 1a, trace (▲)), TiO_2 photocatalysis leads to important MDA accumulation compared with the photo-Fenton process that seems to be produced from inactivated and dead bacteria for both processes.

To detect the reactive oxygen species generated on the surface of the catalyst under illumination with simulated solar light, the ESR spin trap technique with DMPO was used. In particular, DMPO scavenges both •OH and $O_2^{\bullet -}$ radicals, thus leading to the formation of spin-adducts, DMPO–OH or DMPO–OOH, respectively. Both resulting paramagnetic products reveal distinct and easily recognizable ESR spectra. However, the DMPO–OOH spin adduct is well known to be highly unstable and rapidly decomposes into the DMPO–OH spin adduct [25]. Therefore, as a result, a characteristic ESR spectrum of the DMPO–OH spin adduct consisting of four well resolved peaks (1:2:2:1 quartet, $a_N = a_H = 14.9$ G) is usually observed (insert in Fig. 2). In fact, such ESR spectra were observed for all of the studied photo-catalytic systems after exposure to simulated solar light, highlighting their ability to generate both •OH and $O_2^{\bullet -}$ radicals.

Fig. 2 summarizes the ESR spin-trapping experiments for TiO_2 photocatalysis and $FeSO_4$ and goethite-based photo-Fenton systems. The intensity plots of the ESR signal of DMPO–OH as a function of illumination time represent the photocatalytic efficiency of the studied systems. The steepest slope of the DMPO–OH intensity plots was observed for TiO_2 (trace (▲) in Fig. 2). The corresponding time-evolution of acquired ESR signals is shown in the insert to Fig. 2. Note that no ESR signals of DMPO–OH were detected before illumination in this experiment. These results suggest that exposure to the simulated solar light was essential for generation of reactive oxygen species, including •OH, on the surface of the TiO_2 photocatalyst. This phenomenon also points to a classical mechanism of the light-induced promotion of valence band electrons to the conduction band, which yields valance band holes (h_{vb}^+) and produces •OH radicals at the particle surface. The high efficiency of the photo-generation of ROS in the presence of the TiO_2 photocatalyst corroborates with the observed high rate of lipid peroxidation in *E. coli* cells exposed to the photo-catalytic action of this catalyst (Fig. 1a, trace (▲)). Thus, •OH radicals, along with other ROS, such as $O_2^{\bullet -}$, and H_2O_2 generated on the illuminated TiO_2 surface, can attack polyunsaturated phospholipids in *E. coli* cell membranes, leading to their breakdown and cell death [15]. Additionally, h_{vb}^+ of the catalyst can disturb cell membranes, leading to oxidative stress and, eventually, cell death (Fig. 1b, trace (▲)). These findings show that the TiO_2 photocatalyst was highly efficient in the inactivation of *E. coli* under simulated solar light even if TiO_2 utilizes only 4% of the solar spectrum and cannot efficiently utilize visible light which is approximately 43% of the solar spectrum for photocatalytic disinfection.

The oxidative species were also generated by $FeSO_4$-based photo-Fenton systems, as shown in Fig. 2 trace (♦). Interestingly, for the $FeSO_4$-based photo-Fenton system, a small ESR signal of DMPO–OH resulting from the Fenton process in the dark was already observed before illumination. This ESR signal markedly increased on illumination with simulated solar light (Fig. 2, trace (♦)). The observed difference in the extent of lipid peroxidation found between the photo-catalytic action of TiO_2 and the $FeSO_4$ based photo-Fenton system (Fig. 1a, traces (▲) and (♦)) is attributed to the cellular charge effect that may facilitate the adsorption of bacteria cells to TiO_2 particles, leading to the production of •OH close to bacteria affecting the cell wall lipopolysaccharides [14]. The adsorption of bacteria on TiO_2 and the photocatalytic reactivity of TiO_2 are affected by the pH of the suspension. In an experiment involving the TiO_2 photocatalyst, the pH decreased from 6.5 to 5.0 (Table 1). This concomitant decrease in pH is the result of (i) generation of aliphatic acids during photocatalytic oxidation of bacteria and (ii) production of protons [26].

Because the isoelectric point (IEP) of titania is between 6.5 and 7.0 and the pH decreased during the treatment, the density of $TiOH_2^+$ groups increased in the solution and the TiO_2 surface becomes positively charged.

Gumy et al. [27] investigated the electrostatic attraction between the *E. coli* and commercial TiO_2 powders. They observed that the isoelectric point is correlated with the catalytic activity of TiO_2 powders in *E. coli* inactivation. When the TiO_2 surface is positive, the *E. coli* inactivation process was observed to be more efficient. More recently, studies reported by Pigeot-Rémy et al. [17] showed the importance of the cell wall envelope as the primary target of TiO_2 treatment. Even in the dark, the contact between TiO_2

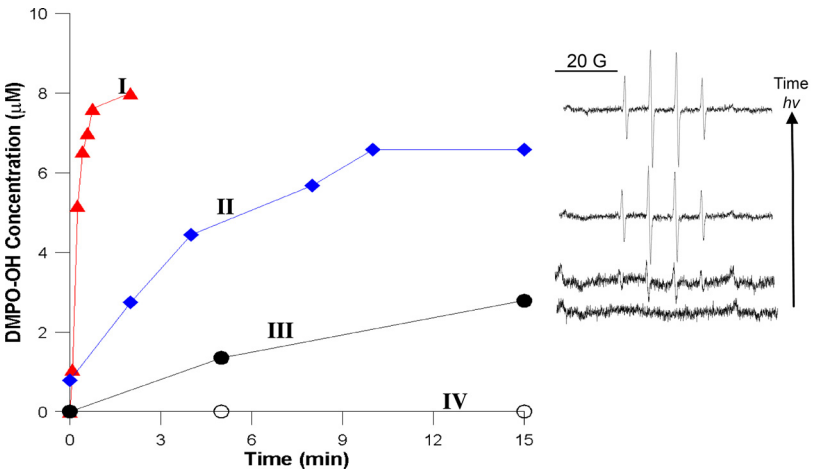

Fig. 2. The ESR-measured formation of hydroxyl radical (OH) in the presence of *E. coli* 10^6 during: (I) (▲) TiO_2 photocatalysis (1 mg/mL); (II) (♦) photo-Fenton ($FeSO_4$ (Fe^{2+} 0.6 mg/L), H_2O_2 (10 mg/L), under light); (III) (●) photo-Fenton (goethite) (0.6 mg/L of added iron ion), H_2O_2 (10 mg/L), under light); (IV) (○) light alone. *Insert*: typical ESR traces of the paramagnetic spin adduct, DMPO–OH for TiO_2 photocatalysis.

and bacteria damages the cell wall. In contrast, contact between *E. coli* and SiO_2 did not induce changes in bacterial permeability which was explained by the different electrostatic charges on the two types of surfaces at the pH of the reaction.

The *E. coli* inactivation under photo-Fenton treatment resulted in accumulation of MDA at time zero with a maximum concentration at 300 min (Fig. 1a, trace (♦)). The low accumulated concentration of MDA found in photo-Fenton processes compared with TiO_2 photocatalysis are similar to levels found when using chemical disinfectants such as ozone, chlorine dioxide, free chlorine, and UV irradiation to inactivate *E. coli*. Cell wall damage was reported to be more pronounced with a strong oxidant (such as ozone), causing delayed diffusion as the oxidant reacts with various cell components. In contrast, damage in the inner cell components was more apparent with weaker oxidants (such as free chlorine) that have limited reactions with cell walls and that reach the cell plasma [28]. This situation may occur for near-neutral photo-Fenton treatment resulting in efficient bacterial inactivation, but that reveals rather limited lipid peroxidation (Fig. 1a, trace (♦)). Control experiments Fe^{2+}/hv; H_2O_2/hv; *hv* alone and Fenton does not significantly contributed to lipid peroxidation (Fig. 1a). However, complete bacterial inactivation was achieved for Fe^{2+}/hv and H_2O_2/hv system controls and 5 log and 2 log reduction of bacteria under light alone and Fenton systems were reached at 420 min of treatment (Fig. 1b). Thus, extensive membrane damage may not be the only pathway in the inactivation of bacteria by photo-Fenton treatment. The intensification of internal (photo)Fenton processes by the synergistic action of UVA light and external Fenton's reactants seem important to bacterial inactivation by near-neutral photo-Fenton.

Although the initial Fe^{2+} added to the solution was 0.6 mg/L, the concentration of total dissolved iron measured at time 0 min was 0.3 mg/L, 0.2 mg/L at 60 min, and negligible beyond 60 min of treatment (Table 2). This loss of dissolved iron may be provoked by (i) the iron precipitation as ferric (hydr)oxide attributable to near-neutral pH (Table 1) [29], (ii) adsorption on the bacterial wall, and (iii) Fe^{2+} intake by bacteria. Thus, after 60 min of treatment (Fig. 1b, trace (♦)), *E. coli* inactivation could be mediated by heterogeneous photocatalytic action of solid iron species as iron (hydr)oxide, mostly goethite (α-FeO(OH)) and/or lepidocrocite (γ-FeO(OH)) that could be formed by oxidation of Fe^{2+} in solution at near-neutral pH [29]. This result corresponds to previous findings by Nieto-Juarez et al. [11] who showed that inactivation of MS2 coliphage in a Fenton-like system at pH 6.8 was mediated by iron colloids rather than dissolved iron. Thus, this study, evaluates the photocatalytic activity of goethite toward bacterial inactivation during photo-Fenton treatment and compared with the photo-Fenton treatment using cationic iron ($FeSO_4$).

Fig. 3 (traces (♦) and (●)) shows complete *E. coli* inactivation for both $FeSO_4$ and goethite-based photo-Fenton systems before 90 min of treatment. The inactivation rate for photo-Fenton treatment with iron sulfate was more rapid before 60 min compared

Table 1
Initial (i) and final (f) values of pH and H_2O_2 for various systems.

Systems under simulated solar light	pH_i	pH_f	H_2O_{2i}	H_2O_{2f}
Fig. 1a and b				
Photo-Fenton: $FeSO_4$ (Fe^{2+} 0.6 mg/L), H_2O_2 (10 mg/L), *hv*	6.7	6.1	10.0	0.5
TiO_2 photocatalysis (1 mg/mL)	6.5	5.0	–	–
Fig. 3				
Photo-Fenton: $FeSO_4$ (Fe^{2+} 0.6 mg/L), H_2O_2 (10 mg/L), *hv*	6.5	6.0	10.0	6.0
Photo-Fenton: Goethite (Fe^{3+} 0.6 mg/L), H_2O_2 (10 mg/L), *hv*	6.5	6.1	10.0	8.8
Goethite, under light without H_2O_2 (Fe^{3+} 0.6 mg/L), *hv*	6.5	6.3	–	–
Fig. 4				
TiO_2 photocatalytic (1 mg/mL)	6.8	5.2	–	–
Photo-Fenton: $FeSO_4$ (Fe^{2+} 0.6 mg/L), H_2O_2 (10 mg/L), *hv*	6.8	6.4	10.0	5.2
Fig. 6a and b				
$FeSO_4$ (Fe^{2+} 12 mg/L), *hv*	5.7	5.3	–	–
$FeCl_3$ (Fe^{3+} 12 mg/L), *hv*	5.4	4.7	–	–
Fig. 7a and b				
Photo-Fenton: $FeSO_4$ (Fe^{2+} 0.6 mg/L), H_2O_2 (10 mg/L), *hv*	6.5	5.6	10.0	0.4
TiO_2 photocatalysis (1 mg/mL)	6.2	5.1	–	–

Table 2
Evolution of total dissolved iron (Fe^{tot} mg/L) for various systems.

Systems	Time of reaction (min)				
	0	60	120	180	300
Fig. 1a and b					
Photo-Fenton: $FeSO_4$ (Fe^{2+} 0.6 mg/L), H_2O_2 (10 mg/L), *hv*	0.3	0.2	0.0	0.0	0.0
Fig. 3					
Photo-Fenton: $FeSO_4$ (Fe^{2+} 0.6 mg/L), H_2O_2 (10 mg/L), *hv*	0.4	0.2	0.0	–	–
Photo-Fenton: Goethite (Fe^{3+} 0.6 mg/L), H_2O_2 (10 mg/L), *hv*	0.0	0.0	0.0	–	–
Goethite (Fe^{3+} 0.6 mg/L), *hv*	0.0	0.0	0.0	–	–
Goethite (Fe^{3+} 0.6 mg/L), dark	0.0	0.0	0.0	–	–
Fig. 4					
$FeSO_4$ (Fe^{2+} 0.6 mg/L), H_2O_2 (10 mg/L), *hv*) pH 7.0	0.4	0.4	0.3	0.1	0.0
Fig. 7a and b					
Photo-Fenton: $FeSO_4$ (Fe^{2+} 0.6 mg/L), H_2O_2 (10 mg/L), *hv*	0.3	0.1	0.0	0.0	0.0

with goethite. A 3 $\log_{10}$ reduction (99.8%) of the initial *E. coli* concentration was achieved after 60 min (Fig. 3, trace (♦)), suggesting a significant contribution by a homogenous photo-catalytic reaction (Eq. (1)) because dissolved iron was present before 60 min of treatment (Table 2). Thus, after 60 min of treatment a transition from a homogenous to a heterogeneous process occurred (see Table 2) and *E. coli* inactivation was mediated by the heterogeneous photocatalytic action of solid iron species that participated in the (photo)Fenton reactions, although at slower rates than dissolved iron [29]. When goethite was added from the beginning of the treatment under the simultaneous presence of light and H_2O_2, total *E. coli* inactivation was reached at 90 min of treatment (Fig. 3, trace (●)) and total dissolved iron was not detected in the filtrate samples during the reaction performed at pH 6.5 (Table 2). Thus, *E. coli* inactivation was mediated by a heterogeneous photo-Fenton process from the beginning of the reaction. Therefore, the following steps explain the inactivating effect of goethite.

(1) The enhanced adsorption of *E. coli* cells onto goethite favors the subsequent attack. The pH value of 6.5 (Table 1) used in the experiment is lower than the isoelectric point of goethite (IEP = 7.6–8.9) [30,31], indicating that hydroxyl groups at the surface are partially protonated. Protonated hydroxyl groups bound to lattice Fe^{3+} may be represented by $>Fe\text{-}OH_2^+$, where the symbol $>$ denotes a surface-bound species. The surface interaction of $>Fe\text{-}OH_2^+$ with *E. coli* is favored by electrostatic attraction forces because the *E. coli* surface is negative charged between pH 3 and pH 9 because of phospholipids and lipopolysaccharides on its cell surface [15]. Thus, the contact/attraction of $>Fe\text{-}OH_2^+$ with *E. coli* is favorable in accelerating inactivation kinetics. The adsorption of gram-negative bacterium on goethite and iron oxides has been demonstrated [30,32]. However, as is shown in Fig. 3 (trace (+)), negligible inactivation of *E. coli* was observed using the goethite/dark system, indicating that the adsorption of iron (hydr)oxide particles on bacteria does not affect significantly bacterial cultivability after 120 min of treatment.

(2) Semiconductor photocatalytic character of goethite. Iron (hydr)oxide shows semiconductor properties with a narrow band gap of 2.0–2.3 eV and may be photoactive under solar irradiation [33]. Electrons and holes that are photogenerated in the iron oxide semiconductor lattice are scavenged by surface sites ($>FeOH$) to produce $^{\bullet}OH$ radicals and $>Fe^{2+}$.

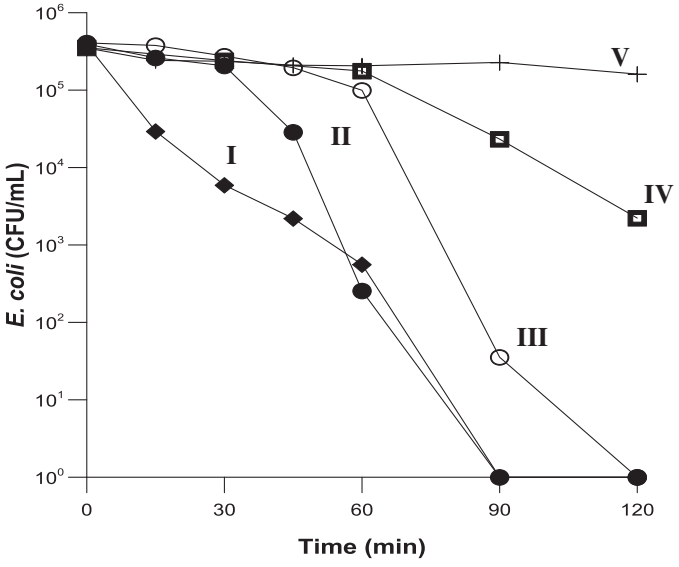

Fig. 3. *E. coli* inactivation during: (I) (♦) photo-Fenton ($FeSO_4$ (Fe^{2+} 0.6 mg/L), H_2O_2 (10 mg/L), under light); (II) (●) photo-Fenton (goethite) (0.6 mg/L of added iron ion), H_2O_2 (10 mg/L), under light); (III) (○) goethite (0.6 mg/L of added iron ion), under light; (IV) (□) light alone; (V) (+) goethite under dark. Experiments were conducted in triplicate and standard error was found to be approximately 5%.

Therefore, the reactive $^{\bullet}OH$ radicals formed during these processes at the goethite and/or from direct oxidation of bacteria by surface holes could contribute to achieving complete bacterial inactivation after 120 min of treatment for the goethite/*hv* system (Fig. 3, trace (○)).

The major efficiency of the goethite/*hv* system in the presence of H_2O_2 (Fig. 3, trace (●)), can be explained because H_2O_2 is an electron acceptor and leads to the formation of additional $^{\bullet}OH$ radicals. The excited electrons photogenerated in the iron oxide photoconductor lattice are directly trapped by the H_2O_2 of the solution to produce $^{\bullet}OH$ radicals (Eq. (5)), that directly attack bacteria adsorbed to the goethite surface.

$$H_2O_2 + e_{cb-} \rightarrow OH^- + {}^{\bullet}OH \quad (5)$$

(3) Heterogeneous mechanism. H_2O_2 initiates a chain reaction that leads to the formation of $^{\bullet}O_2H$ by contact with Fe^{3+} sites available on the surface of goethite particles dispersed in aqueous solution [34]. Concomitantly Fe^{3+} is reduced to Fe^{2+}. New Fe^{2+} reaction sites are then formed and allow H_2O_2 to generate $^{\bullet}OH$ radicals when the Fe^{3+} sites are recovered through oxidation of Fe^{2+} in the cyclic mechanism (Eqs. (6) and (7)).

$$>Fe^{3+}\text{–}OH + H_2O_2 \rightarrow >Fe^{2+} + HO_2{}^{\bullet} + H_2O \quad (6)$$

$$>Fe^{2+} + H_2O_2 \rightarrow >Fe^{3+}\text{–}OH + {}^{\bullet}OH + H_2O \quad (7)$$

$$HO_2{}^{\bullet} \leftrightarrows H^+ + O_2{}^{\bullet-} \quad (8)$$

$$>Fe^{3+}\text{–}OH + HO_2{}^{\bullet}/O_2{}^{\bullet-} \rightarrow >Fe^{2+} + H_2O/OH^- + O_2 \quad (9)$$

$$>Fe^{3+}\text{–}OH + H_2O_2 + hv \rightarrow >Fe^{2+} + H^+ + {}^{\bullet}OH \quad (10)$$

The oxidation ability of the Fenton's reaction (Eqs. (6) and (7)) in a heterogeneous system can be greatly enhanced through the photo-Fenton reaction (Eq. (10)). Thus, the additional radicals photogenerated from Eqs. (5)–(10) contributed to total bacterial inactivation at 90 min of treatment under the heterogeneous photo-Fenton process. As Fig. 2 trace (●) shows, the growth of the ERS signal intensity of DMPO–OH confirms the generation of $^{\bullet}OH$ and $O_2^{\bullet-}$ radicals from a goethite-based photo-Fenton system during *E. coli* inactivation under illumination using simulated solar light. Han et al. [35] also noted this process and revealed that a goethite/H_2O_2 system under room light generated $^{\bullet}OH$ radicals and singlet oxygen.

(4) The heterogeneous action mode of solid goethite can be completed through a homogeneous contribution resulting from photodissolution of goethite promoted by siderophores. Siderophores secreted by many bacteria (for example, ferritins and aerobactin from *E. coli*) [36] were shown to significantly increase the light-induced dissolution of goethite and other ferric (hydr)oxides [37]. The effect of siderophores in the light-induced redox cycling of dissolved iron is dominated by photo-reduction of certain Fe^{3+}-siderophore complexes resulting in the formation of Fe^{2+}. According to Borer et al. [38], the possible Fe^{3+} photo-reduction mechanisms at the iron oxide surface in the presence of siderophores are (i) photolysis of Fe^{3+}-siderophore complexes, which leads to the formation of Fe^{2+}, or (ii) a semiconductor charge transfer mechanism with subsequent migration of the generated photoelectron to the oxide surface. However, in our experiments, no dissolved iron was detected, suggesting a fast reoxidation of surface Fe^{2+} in the presence of oxygen at near-neutral pH and/or rapid Fe^{2+} oxidation by hydrogen peroxide. The latter reaction participates in the catalytic cycle of the (photo) Fenton's reagent, generating additional ROS and leading to bacterial inactivation (Fig. 3, trace (●)). Concomitantly, more than one order of magnitude of H_2O_2 was consumed during the reaction (Table 1). Absence of detection of dissolved iron in the bulk of the solution could be related with the detection limit of the used analytical method (2 μg/L).

3.2. Lipid peroxidation using lipopolysaccharide (LPS)

To test whether MDA was indeed a product of bacterial lipid peroxidation, pure LPS, a component of bacterial wall [39], was used as a model target and was exposed to both photo-Fenton and TiO_2 photocatalysis. Fig. 4 (trace (▲)) shows that MDA levels started to increase to a maximum value of 50 nmol/mg LPS at 30 min, indicating that important peroxidation of membrane lipid was occurring with TiO_2 treatment. For near-neutral photo-Fenton treatment under simulated solar light, low MDA accumulation (maximal concentration of 2.5 nmol/mg before 300 min of treatment) was detected compared with TiO_2 treatment (Fig. 4, trace (▲)). Dissolved iron was observed until 180 min of treatment (Table 2), probably resulting from the LPS chelating effect that favors the maintenance of iron in solution, even a near-neutral pH (Table 1). Modest lipid peroxidation, even on relatively high concentrations of pure LPS, support the hypothesis that this pathway is not the only one in bacterial inactivation and death by photo-Fenton treatment at near-neutral pH. In each experiment, a residual peroxide concentration was detected at the end of the experiments, ensuring that a photo-Fenton reaction occurred during entire treatment period (Table 1).

3.3. MDA degradation

Lipid product MDA is known as a target of oxidative degradation. Thus, to assess the extent of the oxidative degradation

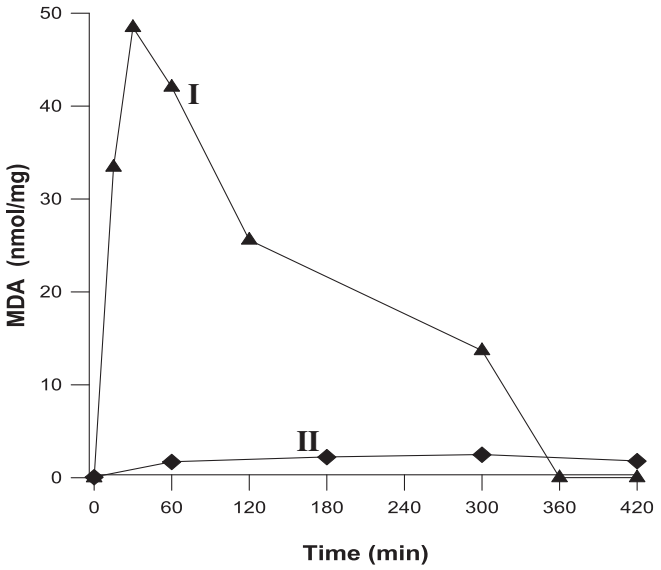

Fig. 4. Lipid peroxidation based on MDA accumulation on LPS (0.4 mg/L) during: (I) (▲) TiO_2 photocatalysis (1 mg/mL); (II) (♦) photo-Fenton ($FeSO_4$ (Fe^{2+} 0.6 mg/L), H_2O_2 (10 mg/L), under light). Experiments were conducted in triplicate and standard error was found to be approximately 5%.

of MDA under both photocatalytic treatments, different MDA solutions (2.0 nmol/mL) were treated for 30 min with both TiO_2 photocatalysis and photo-Fenton process. The residual amount of MDA was determined using the same analytic method of HPLC (Fig. 5, trace (▲)) shows that MDA was oxidatively destroyed within 10 min by TiO_2 photocatalysis, whereas the degradation kinetic for photo-Fenton treatment was slower (longer than 20 min) (Fig. 5, trace (▲)). These results indicate that MDA under photo-catalytic conditions is a relatively unstable product that undergoes further metabolic transformations. MDA has two aldehyde groups, and the degradation products are expected to be ring cleavage products, such as malonic semialdehyde, malonate, monoaldehydes (formaldehyde, acetaldehyde), monoketons (acetone), and

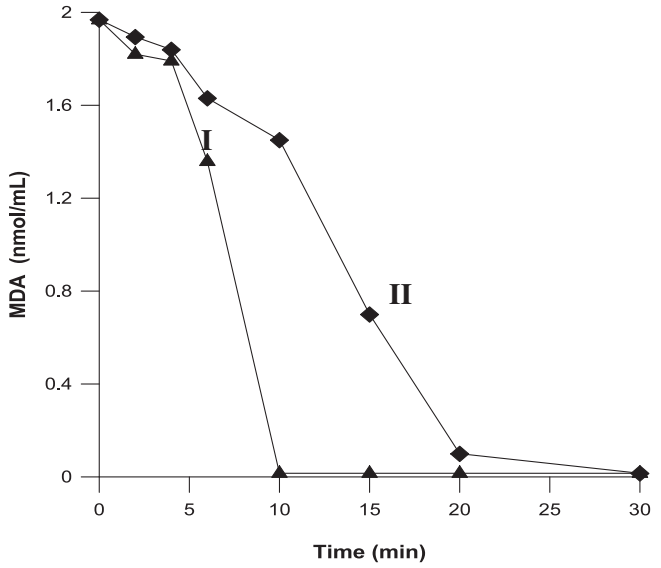

Fig. 5. MDA degradation during: (I) (▲) TiO_2 photocatalysis (1 mg/mL); (II) (♦) photo-Fenton ($FeSO_4$ (Fe^{2+} 0.6 mg/L), H_2O_2 (10 mg/L), under light). Experiments were conducted in triplicate and standard error was found to be approximately 5%.

carboxylic acids (formic and/or acetic acid), or complete mineralization products such as CO_2, and H_2O [40]. Therefore, the MDA values in each peroxidation lipidic experiment are the net result of its production and photocatalytic degradation in oxidative conditions. Thus, eventually, the rate of MDA degradation exceeds the rate of MDA production, as observed after 300 min of reaction in the TiO_2 photocatalysis, and photo-Fenton treatment on bacteria (Fig. 1a, trace (▲)) and 30 and 300 min on LPS (Fig. 4 (traces (▲)) and (♦)). Although the TiO_2 photocatalysis treatment degrades MDA at higher rates, its accumulation during lipid peroxidation was also higher when compared with the photo-Fenton treatment with a similar disinfection efficiency (Fig. 1a, traces (▲)) and (♦)).

3.4. Different bacterial inactivation mechanisms depending on the use of Fe^{2+} or Fe^{3+}

Several studies reported that extracellular Fe^{2+} can penetrate into the cell or react with oxygen, leading to the formation of ROS under light [41,42]. At near-neutral pHs, Fe^{3+}-organo complexes are able to play an important role in the photogeneration of •OH radicals that attack cellular membranes, causing lipid peroxidation. Because we used Milli-Q water, these Fe-organo complexes are formed by by-products generated from bacteria degradation and lysis. Therefore, we evaluated the effect of Fe^{2+} and Fe^{3+} under simulated solar light on lipid peroxidation during bacterial inactivation. As Fig. 6a (traces (■) and (●)) shows, higher

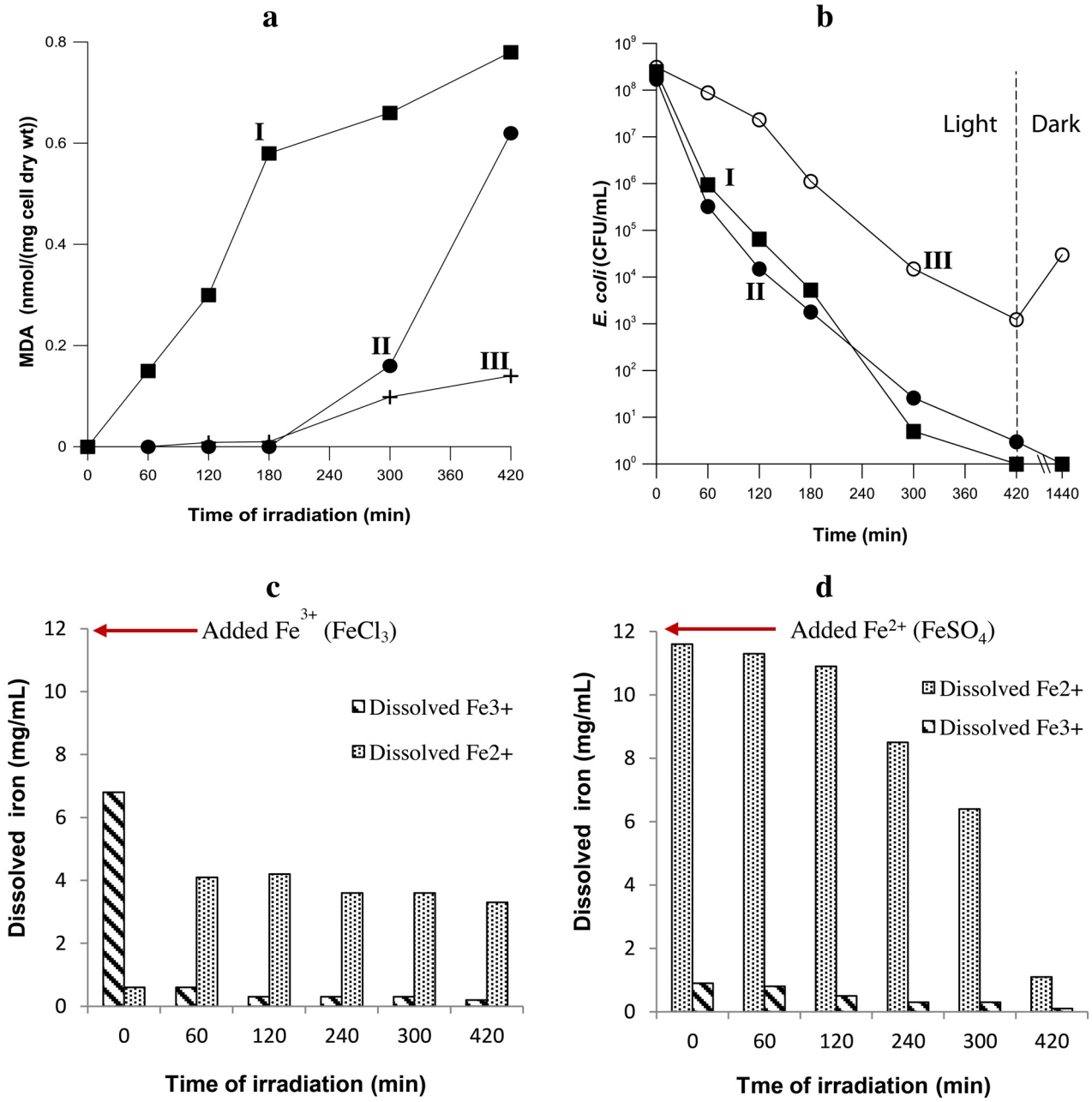

Fig. 6. (a) Lipid peroxidation based on MDA accumulation. (b) *E. coli* inactivation, during: (I) (■) $FeCl_3$ (Fe^{3+} 12 mg/L), under light; (II) (●) $FeSO_4$ (Fe^{2+} 12 mg/L), under light; (III) (+) light alone. (c) Evolution of dissolved iron (Fe^{2+}, Fe^{3+}) after filtration during photo inactivation of *E. coli* suspended in a solution of $FeCl_3$ (Fe^{3+} 12 mg/L). (d) Evolution of dissolved iron (Fe^{2+}, Fe^{3+}) after filtration during photo inactivation of *E. coli* suspended in a solution of $FeSO_4$ (Fe^{2+} 12 mg/L). H_2O_2 was not added. Experiments were conducted in triplicate and standard error was found to be approximately 5%.

MDA accumulation was observed for the treatment initiated with Fe^{3+}/*hv* compared with Fe^{2+}/*hv* system. Nevertheless, the inactivation rates for both photo-treatment methods were similar with a 7 $\log_{10}$ reduction in *E. coli* concentration reached after 5 h (Fig. 6b, traces (■) and (●)). The significant MDA accumulation observed with Fe^{3+} under simulated solar light is probably the result of Fe^{3+} binding to proteins of the bacterial membrane and their carboxylic endgroups forming Fe^{3+}-bacteria complexes. The photo-reduction of these complexes under UVA and visible radiation, leads to a reduction of Fe^{3+} to Fe^{2+} and oxidation of the chelating ligand *via* ligand-to-metal charge transfer (LMCT) [6]. Both, Fe^{2+} and ligand radicals react with O_2, forming ROS ($O_2^{\bullet-}$, $^{\bullet}OH$, H_2O_2) close to the target bacteria and leading to lipid peroxidation chains [43] and bacterial inactivation (Fig. 6b, trace (■)), for example, because of increased permeability and/or the disruption of trans membrane ion gradients [4,19,44].

To manage the transport of Fe^{3+} into the cell, *E. coli* elaborate and secrete high affinity extracellular ferric chelators called siderophores to solubilize iron prior to transport [45]. The first step in the internalization process (for Gram-negative bacteria) requires outer membrane (OM) receptor proteins that bind cognate ferri-siderophores with high specificity to transfer iron into the cytoplasm. Once internalized, this process is thought to involve reduction of the siderophore-associated iron resulting in oxidized siderophore dissociation attributable to the relatively low affinity of siderophores for Fe^{2+}. Thus, into the cell, Fe^{2+} can react with metabolic H_2O_2 to generate internal $^{\bullet}OH$ radicals. However, the internal photo-Fenton reaction promoted by the siderophores penetration of Fe^{3+} and its subsequent delivery as Fe^{2+} is considerably less rapid than that originating from the direct penetration of Fe^{2+} forms because Fe^{3+}-siderophore is used for facultative respiration by *E. coli* [44]. Thus, understandably, the bactericidal effect of Fe^{3+} for this mechanism is intuitively less pronounced than for Fe^{2+}. Hence, the *E. coli* inactivation observed for Fe^{3+} under light in Fig. 6b (trace (■)) could be mediated principally by the ROS generated by the photosensitization of Fe^{3+}-bacteria complexes and Fe^{3+}-siderophore complexes [38]. The formation of these complexes with bacteria can be corroborated through the detection of dissolved ferric species using the Ferrozine method even at pH 5.4 (Fig. 6c, trace (▨)) in which the ferric species are complexed and, thus, solubilized by internal bacteria components [46]. However, the dissolved ferric species decrease further in the treatment. The quasi-stationary concentrations observed for dissolved Fe^{2+} and Fe^{3+} in photocatalytic redox cycle after 120 min to 300 min in Fig. 6c, trace (▨) result from Fe^{2+} generation by photo-reduction of Fe^{3+}-bacteria, Fe^{3+}-siderophore, and Fe^{3+} by-product complexes from one side and the oxidation of Fe^{2+} by O_2 on the other side. In contrast, part of the Fe^{3+} precipitates as insoluble Fe-(hydr)oxides at the experimental pH (Table 1) because an average of 54% of total dissolved iron was lost and could stick to reactors walls, the magnetic stirrer, and on bacteria.

The photo-inactivation rate observed in the treatment initiated with Fe^{2+} under light (pH 5.7) (Fig. 6b (trace (●)) is the result of intracellular Fenton's reactions because added Fe^{2+} can diffuse freely into cells given a lower charge density compared with Fe^{3+}, and it is enhanced by favorable osmotic forces present in Milli-Q water [19,47]. Additionally, Fe^{2+} can be transported into the cytoplasmic membrane through specific proteins, essential for Fe^{2+} uptake in bacteria [42]. Once internalized, Fe^{2+} leads to the generation of $^{\bullet}OH$ radicals when reacting with metabolic H_2O_2 accumulated once catalase is inactivated by UVA radiation [44]. Even though MDA accumulation was not detected in the presence of Fe^{2+} before 180 min of treatment (Fig. 6a, trace (●)), 5 $\log_{10}$ of the initial *E. coli* concentration was inactivated at this time (Fig. 6b, trace (●)). This result indicates that, under light treatment, and in contrast to Fe^{3+}, Fe^{2+} does not significantly contribute to lipid peroxidation to inactivate bacteria. MDA accumulation begun to be detected only after 180 min of treatment (Fig. 6a, trace(●)) because Fe^{2+} goes in, becomes Fe^{3+}, and targets the cell membrane. Further in the treatment, a significant concentration of dissolved ferrous species was observed during the treatment (Fig. 6d, trace (▨)), favored by (i) the formation of complexes with by-products generated from bacterial inactivation that may help Fe^{2+} solubilization, and (ii) the pH because at near-neural pH, soluble iron species such as $[Fe]^{2+}$, $[Fe(OH)]^{+}$ and $[Fe(OH)_2]$ are formed in the aqueous system, and the $[Fe(OH)_2]$ species dominates before undergoing subsequent oxidation by O_2 [48]. In our cases, the oxidation rate could be reduced through the high concentration of Fe^{2+} in the solution because the amount of dissolved oxygen is inversely proportional to the iron content of the water [49].

Under simulated light irradiation, a 5 $\log_{10}$ *E. coli* reduction was reached in 420 min of irradiation, as shown in Fig. 6b (trace (○)). Thermal inactivation can be excluded because temperatures did not exceed 38 °C [50]; therefore, inactivation was predominantly the result of optical effects. A part of the observed photo-inactivation in Milli-Q water could be the result of the endogenously generated ROS. The excited endogenous photosensitizer may react directly with cellular biomolecules, including the attack of proteins and cell membrane components [51], leading to lipid peroxidation chains as was observed after 180 min of treatment (Fig. 6a, trace (○)) and cell inactivation.

To further evaluate the bactericidal effect of simulated solar light in the presence or absence of Fe^{2+} after stopping illumination, post-irradiation events were monitored during 24 h of subsequent dark storage. As shown in Fig. 6b (trace (○)) in the dark, bacterial reactivation and/or growth of bacteria occurs for bacteria treated with simulated solar light. After 24 h, 1 $\log_{10}$ in bacterial counts were obtained. For the photo-assisted Fe^{2+} treatment (Fig. 6b, trace (●)), no reactivation and/or growth of bacteria was observed and a delayed disinfection effect was observed to continue in the dark. These results are interesting because no addition of hydrogen peroxide is needed and iron naturally present or added in water can act as a low-cost "photocatalyst" for solar water disinfection.

The literature described the efficiency of the Fe^{2+} and Fe^{3+} for *E. coli* inactivation using simulated solar light. Previous work demonstrated that in the presence of 0.6 mg/L of Fe^{2+} or Fe^{3+} under light, total bacterial inactivation was reached from 10^6 CFU/mL in 120 and 180 min for Fe^{2+} and Fe^{3+}, respectively [19]. In contrast, no significant differences were observed in our results as a function of the oxidation state of iron. García-Fernández et al. [10] also reported complete *E. coli* inactivation after 15 min (1.2 kJ/L) of solar exposure in the presence of 10 mg/L of Fe^{3+} with total dissolved iron of 1.4 mg/L.

3.5. Disruption of bacteria cell wall by photo-Fenton and TiO_2 photocatalytic action

The ortho-nitrophenyl-β-D-galactoside (ONPG) hydrolysis rate was measured to determine the damage in cell walls during near-neutral photo-Fenton and TiO_2 photocatalysis. Interestingly, in contrast to cellular permeability, the bacterial inactivation experiments mediated by both TiO_2 photocatalysis and photo-Fenton proceeded with similar inactivation kinetics (Fig. 7b, traces (▲) and (♦)). Indeed, the extent of cell damage measured using ONPG concentration was very different for both photo-oxidative treatments (Fig. 7a, traces (▲) and (♦)). The experiment with TiO_2 photocatalysis resulted in an immediate increase in the hydrolytic rate of ONPG with a maximum concentration at 90 min. Suggesting that TiO_2 treatment disrupted the cell wall and/or cytoplasmic membrane, leading to an increase in cell envelope permeability by either an increase in small molecules toward the cell, such as ONPG,

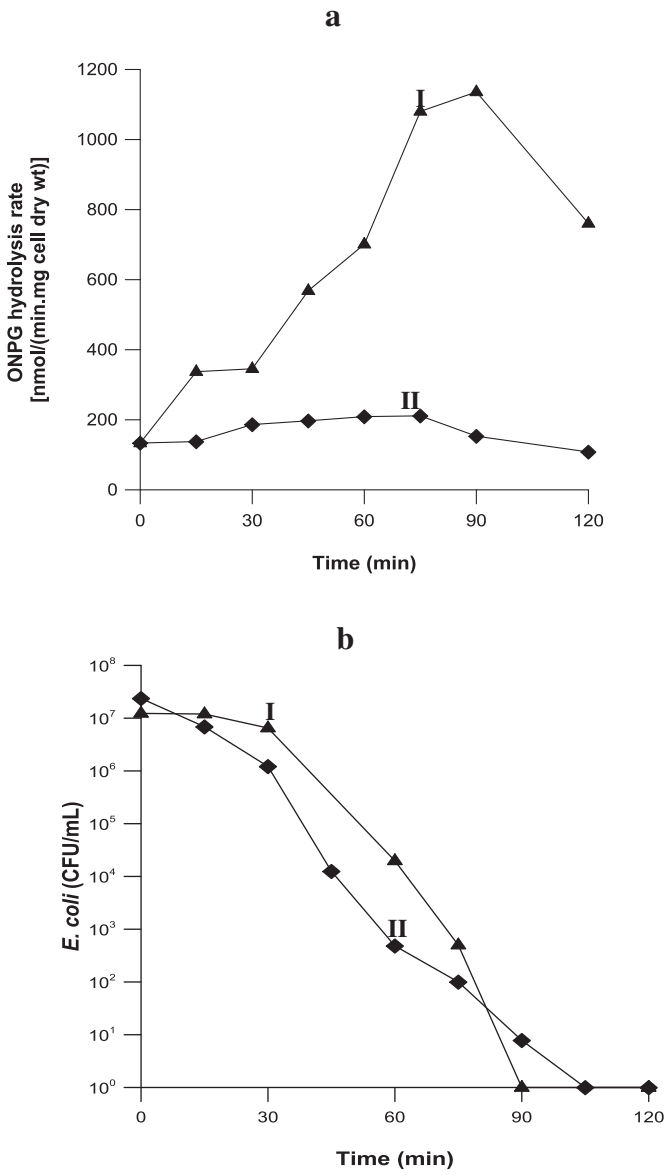

Fig. 7. (a) Cell permeability change based on ONPG hydrolysis rate, (b) *E. coli* inactivation during: (I) (▲) TiO_2 photocatalysis (1 mg/mL); (II) (♦) photo-Fenton ($FeSO_4$ (Fe^{2+} 0.6 mg/L), H_2O_2 (10 mg/L), under light). Experiments were conducted in triplicate and standard error was found to be approximately 5%.

and/or the leakage of large intracellular molecules out of the cell. These results were also consistent with the results of Saito et al., Maness et al., Pigeot et al., and Swetha et al. [14,15,17,52], who confirmed that the cell envelope of *E. coli* is indeed the initial target of TiO_2 photocatalytic reactions and a primary cause of cell death. Under photo-Fenton treatment, a rise in the ONPG hydrolysis rate was observed after 15 min (Fig. 7a, trace (♦)) with a maximum concentration at 75 min of treatment. The corresponding damage of the *E. coli* cell envelope was lower compared with TiO_2 photocatalytic treatment. Thus, although photo-Fenton treatment induced only limited damage to the cell envelope, its overall deleterious effect could be sufficient to disrupt the external structure of bacteria and allow external H_2O_2 and/or iron ions to diffuse into the cell. In the latter case, the internal Fenton's reactions are enhanced to produce powerful oxidative radicals that subsequently degrade intracellular components. These results are indicative of the difference in the extent of cell damage by photo-Fenton and TiO_2 photocatalysis and possibly different mechanisms of bacterial inactivation.

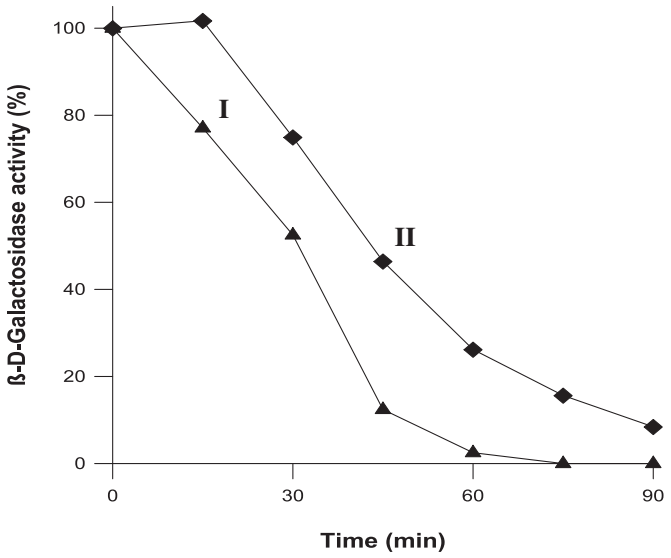

Fig. 8. Effect of various treatments on cell-free β-D-galactosidase activity using cell lysate: (I) (▲) TiO_2 photocatalysis (1 mg/mL); (II) (♦) photo-Fenton ($FeSO_4$ (Fe^{2+} 0.6 mg/L), H_2O_2 (10 mg/L), under light). Experiments were conducted in triplicate and standard error was found to be approximately 5%.

Fig. 7a shows that the ONPG hydrolysis rate declines beyond 75 and 90 min during the photo-Fenton or TiO_2 photocatalysis treatment, respectively suggesting a loss of enzyme activity. Therefore, the effect of both photo-oxidative treatment methods on direct inactivation of cell-free β-D-galactosidase was evaluated using cell lysate. TiO_2 photocatalysis showed a major loss of enzyme activity (90%) compared to photo-Fenton treatment (50%) beyond 45 min of treatment (Fig. 8). However, Fig. 7a shows that whole cells can maintain some level of enzymatic activity indicating that damage to the intracellular content can be precluded at the initial stages by the cell wall and cytoplasmic membrane. This observation confirms the role of the cell envelope as the primary target of TiO_2 attack.

3.6. Mechanistic interpretation of bacterial inactivation at near-neutral pH

Based on these experimental observations and an exhaustive revision of the literature, a mechanistic interpretation of the inactivation of *E. coli* in the presence of Fe^{2+}, Fe^{3+}, H_2O_2, and the photo-Fenton reagent at near-neutral pH under simulated solar radiation is proposed. An overview is presented in Fig. 9. The processes are subdivided in two groups: internal or external processes.

3.6.1. Intensification of internal (photo)Fenton processes by the synergistic action of UVA and external Fenton reactants

(1) UVA light can damage iron-containing proteins such as ferritin, leading to the intracellular release of Fe^{2+} and enzymes, such as catalase or superoxide dismutase (SOD), which constitute a cellular self-defense against ROS [53]. Their disfunction can lead to increased intracellular concentrations of long living ROS such as H_2O_2 and $O_2^{\bullet -}$. [54,55].
(2) Added Fe^{2+} diffuses across the outer membrane and is transported by specific proteins *via* a Feo (ferrous iron-transport) system across the cytoplasmic membrane [47].
(3) Part of the added Fe^{2+} in the bulk of the solution precipitates as iron (hydr)oxides at near-neutral pH and can not move freely into the cell. Thus, siderophores produced by bacteria (enterobactin, aerobactin, and ferrichrome) can chelate iron to manage the Fe^{3+} transport inside the cell for facultative anaerobic respiration *via* siderophores (metabolic Fe^{3+} chelating agents) [37,45]. Fe^{3+} serves as an electron acceptor instead of

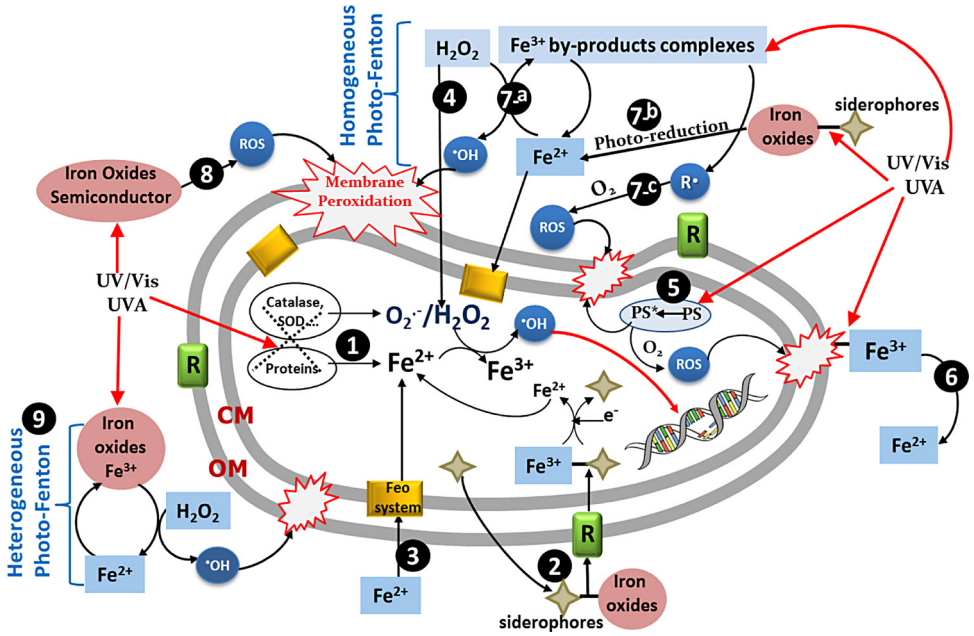

Fig. 9. Mechanistic representation of possible pathways involved in photo-inactivation of *E. coli* in the presence of Fe^{2+}, Fe^{3+} and H_2O_2 at near-neutral pH. R: receptor proteins, CM: cytoplasmatic membrane, OM: outer membrane, PS: photosensitizers.

oxygen in facultative anaerobic respiration of *E. coli*, generating Fe^{2+}.

(4) Added H_2O_2 in the bulk of the solution can penetrate bacterial membrane and diffuses into cells; therefore, H_2O_2 stress arises inside cells [56].

(5) Endogenous cell photosensitizers such as porphyrins, cytochromes, aromatic amino acids, flavins, tryptophan, chlorophyll, and other absorb solar light and lead to ROS generation [57].

The formation or penetration of H_2O_2 and Fe^{2+} in the cytoplasm by these systems (1–4) and endogenous photo-sensitizers lead to oxidative stress through the intracellular Fenton's reaction [55,56], generating highly toxic •OH that can directly attack DNA, thus causing DNA deactivation primarily *via* pyrimidine dimerization and, consequently, cell growth inhibition [58].

3.6.2. Contribution of external pathways to bacteria inactivation

Considering that the cell wall is a protective barrier against environmental stress to microorganisms, the following external events could occur in which the ROS generated leads to membrane peroxidation and increases in the permeability of bacterial cell walls.

(6) Fe^{3+} can be adsorbed or absorbed on proteins of the bacterial membrane, thus leading to the formation of Fe^{3+}-bacteria exciplexes. The photosensitization of these forms by near UVA and visible light might result in direct oxidation of the membrane, initiation of lipid peroxidation chains, and generation of Fe^{2+} and •OH [6].

(7) Highly reactive short-living •OH and other ROS are formed in the bulk of the solution by a homogenous process through the contribution of the following routes (a) Extracellular dissolved Fe^{2+}/Fe^{3+} participles in the homogenous (photo)-Fenton reaction (Eqs. (1) and (3)) generate •OH radicals. (b) At near-neutral pH, Fe^{2+} is oxidized and precipitates as ferric (hydr)oxide. Siderophores secreted by bacteria increase the light-induced dissolution of ferric (hydr)oxide by forming bacteria Fe^{3+}-siderophore complex [36–38]. Additionally, by-products generated from bacterial inactivation can be polydentate ligands that form complexes with ferric ions (Fe^{3+} by-products), allowing their solubilization. The photo-reduction of these complexes under UVA and visible radiation, produce •OH and regenerating Fe^{2+} *via* ligand-to-metal charge transfer (LMCT) [6]. (c) The radical formed by the photosensitization of Fe^{3+} by-products complexes react with O_2 leading to the formation of the radicals $O_2^{\bullet -}/HO_2^{\bullet}$.

(8) A semiconductor effect and/or photoredox reaction is carried out on the iron (hydr)oxide, contributing to the formation of $\equiv Fe^{2+}$ and •OH [33,59].

(9) Heterogeneous photocatalytic action since iron (hydr)oxide was formed during the treatment at the near-neutral pH.

4. Conclusions

The results of lipid peroxidation and permeability change in the cell envelope suggest a mechanism of bacterial inactivation difference for near-neutral photo-Fenton and TiO_2 photocatalysis. The bacterial inactivation mechanism by the photo-Fenton process at near-neutral pH is mediated by both internal and external processes that occur in bacteria. In contrast, for TiO_2 photocatalysis, the cell envelope damage is a significant target. However, further investigations are required to elucidate this aspect.

We propose that the mechanism of bacterial inactivation by photo-Fenton treatment at near-neutral pH is mediated by both internal and external processes. Internal (photo)Fenton processes are mediated by the synergistic action of UVA and external Fenton reactants. For external events, homogenous and heterogeneous photocatalytic actions contributed to efficient bacterial inactivation. Based on the experimental results and a critical revision of the literature, a mechanistic interpretation of near neutral photo-Fenton toward bacterial inactivation is proposed. Fig. 9 presents an overview.

E. coli inactivation rates photo-assisted by the bare presence of Fe^{2+} and Fe^{3+} in the absence of H_2O_2 are similar. However, the specific action mode of each ionic form was not the same. For $Fe^{3+}/h\nu$, the cell membrane damage was more important compared with $Fe^{2+}/h\nu$. Fe^{3+} binds to the cellular membrane and siderophores and generates localized ROS that attack cellular membranes,

causing lipid peroxidation. Conversely, Fe^{2+} can diffuse into the cell through the FeO system and participate in intracellular Fenton's reactions, leading to the generation of •OH radicals when reacting with metabolic H_2O_2 inside the cells. Because iron is naturally present or added in water as Fe^{3+}, the findings of this study are relevant to water disinfection *via* low-cost photocatalysts.

In addition to the mechanistic routes proposed in Milli-Q water, we must consider other additional contributions if the process is performed in natural water. Dissolved organic matter (DOM) present in water can contribute to bacterial inactivation by the action of photo-sensitizer species and/or by complexing with iron, keeping it soluble and becoming part of the photo-Fenton's reaction chain.

Acknowledgements

The authors wish to thank the Swiss National Science Foundation for financial support through the program "Research partnership with developing countries" Project No. IZ70Z0_131312/1-2.

References

[1] A.-G. Rincón, C. Pulgarin, Appl. Catal. B: Environ. 63 (2006) 222–231.
[2] A.-G. Rincón, C. Pulgarin, Catal. Today 124 (2007) 204–214.
[3] A. Moncayo-Lasso, J. Sanabria, C. Pulgarin, N. Benítez, Chemosphere 77 (2009) 296–300.
[4] P. Cieśla, P. Kocot, P. Mytych, Z. Stasicka, J. Mol. Catal. A: Chem. 224 (2004) 17–33.
[5] J.P. Jolivet, C. Chaneac, E. Tronc, Chem. Commun. (Camb.) 338 (2004) 481–487.
[6] W. Feng, D. Nansheng, Chemosphere 41 (2000) 1137–1147.
[7] B.C. Faust, R.G. Zepp, Environ. Sci. Technol. 27 (1993) 2517–2522.
[8] F. Wu, N.S. Deng, Chemosphere 41 (2000) 1137–1147.
[9] A. Bernabeu, R. Vicente, M.A. Peribáñez, A. Arques, A.M. Amat, Chem. Eng. J. 171 (2011) 490–494.
[10] I. García-Fernández, M.I. Polo-López, I. Oller, P. Fernández-Ibáñez, Appl. Catal. B: Environ. 121–122 (2012) 20–29.
[11] J.I. Nieto-Juarez, K. Pierzchała, A. Sienkiewicz, T. Kohn, Environ. Sci. Technol. 44 (2010) 3351–3356.
[12] E. Ortega-Gómez, P. Fernández-Ibáñez, M.M. Ballesteros Martín, M.I. Polo-López, B. Esteban García, J.A. Sánchez Pérez, Water Res. 46 (2012) 6154–6162.
[13] K. Sunada, T. Watanabe, K. Hashimoto, J. Photochem. Photobiol. A: Chem. 156 (2003) 227–233.
[14] T. Saito, T. Iwase, J. Horie, T. Morioka, J. Photochem. Photobiol. B: Biol. 14 (1992) 369–379.
[15] P.C. Maness, S. Smolinski, D.M. Blake, Z. Huang, E.J. Wolfrum, W.A. Jacoby, Appl. Environ. Microbiol. 65 (1999) 4094–4098.
[16] C. Pulgarin, J. Kiwi, V. Nadtochenko, Appl. Catal. B: Environ. 128 (2012) 179–183.
[17] S. Pigeot-Rémy, F. Simonet, E. Errazuriz-Cerda, J.C. Lazzaroni, D. Atlan, C. Guillard, Appl. Catal. B: Environ. 104 (2011) 390–398.
[18] O.K. Dalrymple, W. Isaacs, E. Stefanakos, M.A. Trotz, D.Y. Goswami, J. Photochem. Photobiol. A: Chem. 221 (2011) 64–70.
[19] D. Spuhler, J. Andrés Rengifo-Herrera, C. Pulgarin, Appl. Catal. B: Environ. 96 (2010) 126–141.
[20] F. Karatas, M. Karatepe, A. Baysar, Anal. Biochem. 311 (2002) 76–79.
[21] J. Tsaknis, S. Lalas, V. Tychopoulos, M. Hole, G. Smith, Analyst 123 (1998) 325–327.
[22] Z. Huang, P.-C. Maness, D.M. Blake, E.J. Wolfrum, S.L. Smolinski, W.A. Jacoby, J. Photochem. Photobiol. A: Chem. 130 (2000) 163–170.
[23] H. Esterbauer, K.H. Cheeseman, Methods Enzymol. 186 (1990) 407–421.
[24] N.T.N. Candan, Neurotoxicology 29 (2008) 708–713.
[25] G.R. Buettner, R.P. Mason, Methods Enzymol. 186 (1990) 127–133.
[26] C. Guillard, T.-H. Bui, C. Felix, V. Moules, B. Lina, P. Lejeune, C. R. Chim. 11 (2008) 107–113.
[27] D. Gumy, C. Morais, P. Bowen, C. Pulgarin, S. Giraldo, R. Hajdu, J. Kiwi, Appl. Catal. B: Environ. 63 (2006) 76–84.
[28] M. Cho, J. Kim, J.Y. Kim, J. Yoon, J.H. Kim, Water Res. 44 (2010) 3410–3418.
[29] R.M. Cornell, U. Schewetmann, The iron oxides: Structure, properties, reactions, occurrence and uses, VCH, Weinheim, 2003.
[30] D. Jiang, Q. Huang, P. Cai, X. Rong, W. Chen, Colloids Surf. B: Biointerfaces 54 (2007) 217–221.
[31] C.L. Peacock, D.M. Sherman, Geochim. Cosmochim. Acta 68 (2004) 2623–2637.
[32] H. Wu, D. Jiang, P. Cai, X. Rong, Q. Huang, Colloids Surf. B: Biointerfaces 82 (2011) 147–151.
[33] J.K. Leland, A.J. Bard, J. Phys. Chem. 91 (1987) 5076–5083.
[34] S.-S. Lin, M.D. Gurol, Environ. Sci. Technol. 32 (1998) 1417–1423.
[35] S.K. Han, T.M. Hwang, Y. Yoon, J.W. Kang, Chemosphere 84 (2011) 1095–1101.
[36] S.C. Andrews, A.K. Robinson, F. Rodriguez-Quinones, FEMS Microbiol. Rev. 27 (2003) 215–237.
[37] H.G. Upritchard, J. Yang, P.J. Bremer, I.L. Lamont, A.J. McQuillan, Langmuir 23 (2007) 7189–7195.
[38] P.M. Borer, B. Sulzberger, P. Reichard, S.M. Kraemer, Mar. Chem. 93 (2005) 179–193.
[39] V. Nadtochenko, N. Denisov, O. Sarkisov, D. Gumy, C. Pulgarin, J. Kiwi, J. Photochem. Photobiol. A: Chem. 181 (2006) 401–407.
[40] D.R. Janero, Free Radic. Biol. Med. (1990) 515–540.
[41] C. Catastini, M. Sarakha, G. Mailhot, M. Bolte, Sci. Total Environ. 298 (2002) 219–228.
[42] C.K.Y. Lau, H. Ishida, Z.H. Liu, H.J. Vogel, J. Bacteriol. 195 (2013) 46–55.
[43] E. Cabiscol, J. Tamarit, J. Ros, Int. Microbiol. 3 (2000) 3–8.
[44] V. Braun, Int. J. Med. Microbiol. 291 (2001) 67–79.
[45] W. Köster, Res. Microbiol. 152 (2001) 291–301.
[46] A. Safarzadeh-Amiri, J.R. Bolton, S.R. Cater, J. Adv. Oxid. Technol. 1 (1996) 18–26.
[47] M.L. Cartron, S. Maddocks, P. Gillingham, C.J. Craven, S.C. Andrews, Biometals 19 (2006) 143–157.
[48] B. Morgan, O. Lahav, Chemosphere 68 (2007) 2080–2084.
[49] J.S. Dendy, Determination of Depletion of Dissolved Oxygen Content in Water, United States Patent Office, 1968, Patent Number: 3,375,078 Class: 436.
[50] M. Berney, H.U. Weilenmann, J. Ihssen, C. Bassin, T. Egli, Appl. Environ. Microbiol. 72 (2006) 2586–2593.
[51] M. Gourmelon, J. Cillard, M. Pommepuy, J. Appl. Bacteriol. 77 (1994) 105–112.
[52] S. Swetha, M. Kumari Singh, K.U. Minchitha, R. Geetha Balakrishna, Photochem. Photobiol. 88 (2012) 414–422.
[53] A. Eisenstark, Mutat. Res. 422 (1998) 85–95.
[54] J. Hoerter, A. Arnold, C. Ward, M. Sauer, S. Johnson, T. Fleming, A. Eisenstark, J. Photochem. Photobiol. B: Biol. 79 (2005) 151–157.
[55] J.A. Imlay, Annu. Rev. Microbiol. 57 (2003) 395–418.
[56] J.A. Imlay, Annu. Rev. Biochem 77 (2008) 755–776.
[57] R.H. Reed, Adv. Appl. Microbiol. 54 (2004) 333–365.
[58] R.G. Zepp, B.C. Faust, J. Hoigne, Environ. Sci. Technol. 26 (1992) 313–319.
[59] J. Kiwi, M. Gratzel, J. Chem. Soc.: Faraday Trans. I 83 (1987) 1101–1108.